Journal of Engineering Science and Technology
Vol. 13, No. 6 (2018) 1420 - 1439

CONTROL AND MANAGEMENT OF A SOLAR-WIND HYBRID SYSTEM FOR POWER QUALITY IMPROVEMENT

B. TOUAL[1,3,*], L. MOKRANI[2], A. KOUZOU[3], M. MACHMOUM[4]

[1]Department of Electrical Engineering, University of Batna 2, Algeria
[2]LACoSERE Laboratory, University of Laghouat, Algeria
[3]LAADI Laboratory, University of Djelfa, Algeria
[4]IREENA, 37 Boulevard de l'Université, Bp 406, 44602 Saint-Nazaire, Nantes, France
*Corresponding Author: toualb@gmail.com

Abstract

The main aim of this paper is to present a modified Maximum Power Point Tracking (MPPT) control strategy of a solar-wind hybrid power system, which allows producing a maximum of energy while enhancing the produced power quality by reducing its fluctuation rate. Indeed, the Photovoltaic System (PVS) is based on a PV field of panels connected to the grid through a DC-DC and DC-AC PWM converters and the Wind Energy Conversion System (WECS) is based on a stator field oriented Doubly Fed Induction Generator (DFIG) which its rotor is connected to the network via a back to back AC-DC-AC PWM converter. The proposed control strategy ensures a conventional Maximum Power Point Tracking (MPPT) for the WECS. Furthermore, it guarantees a smooth power injected in the grid by applying a modified MPPT technique applied to the PV system. This strategy uses a part of the PVS available power to compensate the WECS power fluctuations due to wind gusts and generates simultaneously the maximum of smoothed power from the residual part. The simulations results obtained in the case of the proposed control strategy have been compared to those of a conventional MPPT technique and of a Guaranteed Minimum Available Power (GMAP) control strategy. It is obvious that the proposed modified MPPT keeps a good compromise between the quantity and the quality of the total hybrid system produced power.

Keywords: Back to back AC-DC-AC PWM converter, Boost converter, Field oriented DFIG, Power quality improvement, PVS, WECS.

1. Introduction

In recent years, the use of electric hybrid systems has increased in many industrial

Nomenclatures

C_{conv}	Boost capacitor (Fig. 4), F
C_p	Turbine power coefficient
C_S	Reference saturation current $I_{pvsc} / \left(e^{\left(V_{pv0} / (n V_t) \right)} - 1 \right)$, A
d	Duty cycle of the boost converter (Fig. 4)
E_{gap}	Gap energy, depending on the material of the cell, eV
I_{conv}	Boost input current (Fig. 4), A
Ic_{conv}	Boost capacitor current (Fig. 4), A
I_{inv}	Inverter input current (Fig. 4), A
I_{ph}	Photo-current, A
I_{pv}	Photovoltaic current (Fig. 4), A
I_{pvsc}	Cell short-circuit current $I_{pvsc} \approx I_{ph}$, A
I_S	Reverse saturation current of the diode $C_S T^3 e^{\left((-E_{gap} q) / (nTK) \right)}$, A
K	Boltzmann constant, J/K
K_{conv}	Boost converter transistor (Fig. 4)
L_{conv}	Boost converter inductance (Fig. 4), H
L_r	Rotor inductance, H
n	PV cell ideality factor, $1 \leq n \leq 5$
q	Electron charge constant, C
R	Blade radius, m
S	Surface swept by the turbine blades, m²
T	Cell temperature, K
V_{dc}	DC bus voltage of the PVS (Fig. 4), V
V_t	Thermodynamic potential KT/q, V
V_{pv}	Photovoltaic voltage (Fig. 4), V
V_{pv0}	Open circuit voltage, V
v	Wind speed, m/s
v_0	Average component of the wind speed, m/s

Greek Symbols

β	Pitch angle of the turbine blades, deg
λ	Specific speed of the turbine $R\Omega_t / v$
ρ	Air density, kg/m^3
σ	Blondel dispersion coefficient
Ω_t	Turbine rotation speed, rad/s
Ω_e	DFIG rotation speed, rad/s
ω_r	Rotor pulsation (Fig. 7), rad/s

Abbreviations

DC	Direct Current
DFIG	Doubly Fed Induction Generator
GSC	Grid Side Converter
HS	Hybrid System
MPPT	Maximum Power Point Tracking
PVS	Photovoltaic System
WECS	Wind Energy Conversion System

and domestic sectors such as embedded systems, cars, planes, boats, the electrical power supply of different devices (laptops, mobile telephony, mobile players, toys, etc.) and electrical power plants.

In the near future, the use of these hybrid power systems will become more and more important due to their adequacy to industrial developments in several countries and to the reduction in oil production, as well as to the increase of pollution degree related to continuous emissions of dangerous gases [1]. For these reasons, other alternative energy sources that are sustainable and easy to operate have been strongly proposed and investigated in the whole world, such as the solar energy and the wind energy as presented in Table 1 [2, 3]. Therefore, there is an increasing pace of scientific research in the field of hybrid power systems based on renewable energy sources [4-9].

Table 1. Important global indicators for renewable energy in the world [2, 3].

	Unit	2010	2011	2012	2013	2016
Renewable power installed capacity (with hydro)	GW	1250	1355	1470	1560	2017
Renewable power installed capacity (without hydro)	GW	315	395	480	560	921
Solar PV installed capacity	GW	40	71	100	139	303
Wind power installed capacity	GW	198	238	283	318	487
Concentrating solar thermal power installed capacity	GW	1.1	1.6	2.5	3.4	4.8

It can be seen clearly from Table 1 that the WEC and PV systems are becoming important parts of power generation. Their basic energy sources (wind and solar), present the right choice due to the world abundance of windy sites and illuminated sites as well as windy and illuminated sites in a better combination of the weather in the whole world.

In addition, these sources are clean, economic, sustainable, safe, not expensive and easy to operate, especially for the photovoltaic systems, where there is no noise and no additional mechanical requirement.

In the context of a better exploitation of the solar and the wind renewable energy sources, several studies have been presented, where the main aim was the improvement of the used techniques to ensure the maximization of the produced power from such sources while respecting the quality requirement imposed by the network or the consumer demand.

For the PV systems, several previous researches have proposed different solutions to enhance the profitability of these systems by methods such as the improved MPPT technique, which allows a rapid tracking of the maximum power point based on the simultaneous adjustment of the voltage of the panel (Incremental Conductance Algorithm) and the position of the panel. Moreover, the technique which proposes the improvement of the coupling architecture of the photovoltaic panels and the techniques that have been proposed to improve the used static converters and their control techniques [10-15].

In addition, other research studies have been focused on the improvement of the efficiency and the produced energy quality of the wind power systems. These studies use techniques such as the reactive power compensation and the active filtering of harmonic currents generated by nonlinear loads, as well as the control loops improvement to overcome the influence of the inertia on the frequency [16-18].

Kumar and Bhimasingu [19] proposed a new topology of a multilevel modular inverter which is characterized by a decreased DC bus voltage and the elimination of the diodes and the capacitors in comparison with other conventional topologies, where the main aim of this proposed topology was to enhance the produced power of a hybrid system based on renewable energy.

The work presented in this paper focuses mainly on resolving the dilemma of the quantity of produced power by a grid-connected HS while ensuring a high power quality even in presence of wind gusts. Indeed, this studied HS is composed of two systems, the PVS and the WECS that are connected to the power system network according to the topology shown in Fig. 1.

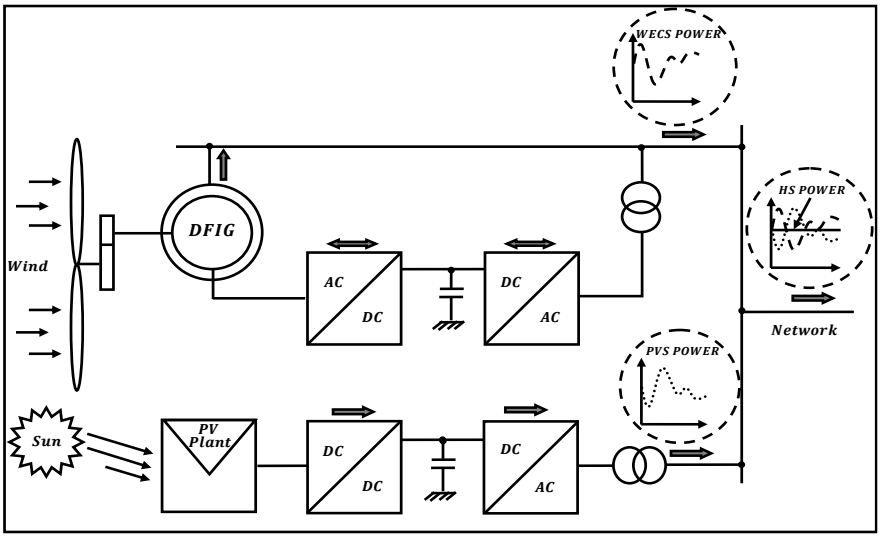

Fig. 1. Description of the studied hybrid system.

The objective of this work is, therefore, the control of the hybrid plant under three operating modes. The first mode is the conventional MPPT mode, where the control system aims to ensure in real time the maximization of the HS total produced power without considering power quality. While the second mode aims to take into account the quality problem of the HS total produced power. In this case, a simple standard decoupled control technique of the HS power is used to produce a maximum smoothed power. The third mode is proposed to ensure the energy production with reduced fluctuations. It is based on a WECS MPPT control, accompanied with the PVS that participates in increasing the overall power production and ensures at the same time the compensation of the WECS produced power fluctuation.

2. Description and Modelling of the PVS

This research study of PVS is based on a solar plant of 400 kW composed of a field of 2000 photovoltaic modules BP SX 3200 (80 parallel branches of 25 modules in series) with a power of 200 Wp for each module [20]. These modules are connected to the power line via a boost converter and a PWM controlled inverter (SOLAR MAX 330 CSV) with a power of 400 kW. This system is equipped with a voltage regulation to control the boost converter in order to ensure a given DC bus voltage at the input side of the inverter. Moreover, the inverter control can ensure a decoupled control of the active and reactive powers (see Fig. 2).

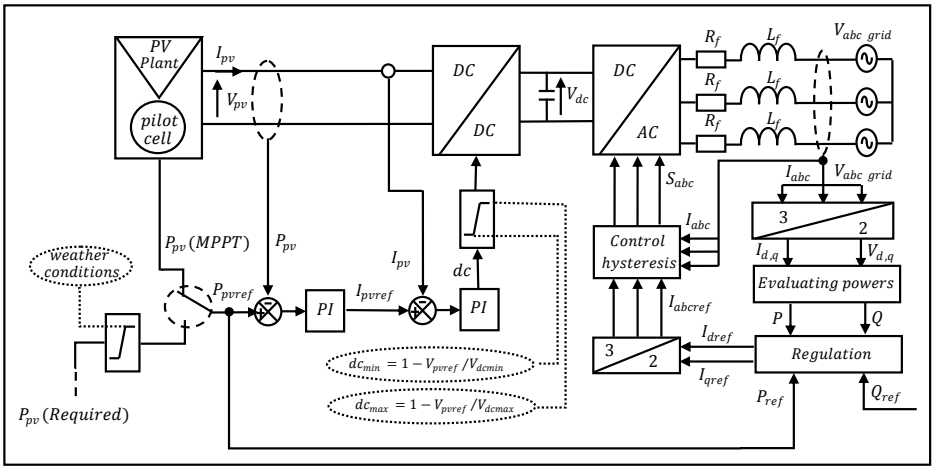

Fig. 2. Description of the photovoltaic studied system.

Indeed, several previous works have focused on the development of different MPPT techniques to optimize the power extraction of photovoltaic sources. All these techniques were based on blind scanning of the MPP. Among these techniques, on can find for example the Perturb and Observe (P.O) technique and its modified version proposed in [21, 22]. However, in the present work, the PVS MPPT control is performed on the basis of an MPP given by a photovoltaic cell implemented in the photovoltaic field to read the meteorological conditions and to generate the reference power to be produced and injected in the network. The boost converter ensures a continuous connection between the PVS and the load (grid) in order to avoid the power waste. Moreover, this converter is controlled in such a way to guarantee an MPPT operation mode, or a given produced power level limited by the weather conditions, whereas, the control of the grid side converter ensures the transfer of this produced power to the grid. The duty cycle value of the boost converter is limited according to the range values (min-max) of the boost converter output voltage (according to input inverter voltage limits).

2.1. Modelling and design of the PV generator

There are many possible mathematical representations with varying complexity that can be used to model the PV cell current-voltage behaviour. However, depending on the application, several factors are required to be taken into account

to obtain a suitable modelling of the PV cell I-V characteristics. In this work, a model with an exponential and four parameters (L4P) is used. Indeed, this model has been widely used. It considers the photovoltaic cell as a dependent current source of illumination and temperature, connected in parallel with a diode and a shunt resistance R_{sh} and a series resistance R_{ser}, (see Fig. 3).

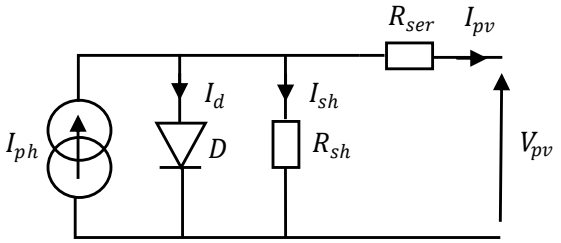

Fig. 3. Equivalent diagram of an L4P cell.

Based on simplification of the parallel resistance which has generally an important value (I_{sh} very small), the current given by the photovoltaic cell can be expressed as follows [23, 24]:

$$I_{pv} = I_{ph} - I_S \left(e^{\left((V_{pv}+I_{pv}R_{ser}\right)/(V_t n))} - 1\right) \tag{1}$$

To generalize the above equations to be valid for various meteorological conditions temperature and illumination, the short-circuit current and the open circuit voltage of the photovoltaic cell are expressed as follows:

$$\begin{cases} I_{pvsc} = (g/g_r)\left(I_{pvscref} - \mu_c(T - T_r)\right) \\ V_{pv0} = V_{pv0ref} - \mu_v(T - T_r) \end{cases} \tag{2}$$

where: g, T, μ_c, μ_v, $I_{pvscref}$, V_{pv0ref}, g_r, and T_r are respectively, the illumination value, the temperature value, the temperature influence factor on the short-circuit current, the temperature influence factor on the open circuit voltage, the reference of the short-circuit current, the reference of the open circuit voltage, the rated illumination and the rated temperature.

By considering the inverter input voltage range $V_{dc} \in [600,900]$ V, the solar farm produces a maximum power equal to the used inverter rated power (P_{max}= 400 kW) under a voltage not higher than 900 V.

Consequently, the number of modules in series N_s and the number of parallel braches N_p can be calculated as follows:

$$\begin{cases} N_s = V_{dc\max} / V_{op\mathrm{mod}} \\ N_p = P_{\max} / \left(N_s P_{\max \mathrm{mod}}\right) \end{cases} \tag{3}$$

where: V_{dcmax}, V_{opmod} and P_{maxmod} are respectively, the maximum of the DC bus voltage, the optimal value of the PV module voltage and the maximum power of the PV module.

With an optimal modular voltage of 24.5 V and a rated power of 200 Wp in this case, a number of 25 modules in series and a number of 80 parallel branches have been used to build the PV plant subject of our study, which is containing 2000 modules of BP SOLAR SX 3200.

2.2. Boost converter modelling

It is important to clarify that the PV energy is not like a conventional energy source because in a conventional energy source, where the energy which is not delivered to the load is not consumed and remains in the source. In PV energy source, the energy is wasted since it is available for free. Thus by using the boost converter, current flows constantly into the input port of the converter due to use of a parallel switch in its topology. Therefore, in PV system, the energy efficiency of the boost converter may be higher than of the buck converter for example [25].

Figure 4 shows the boost converter circuit topology and its operating principle. This converter is used to achieve the required photovoltaic current tracking based on the switch control.

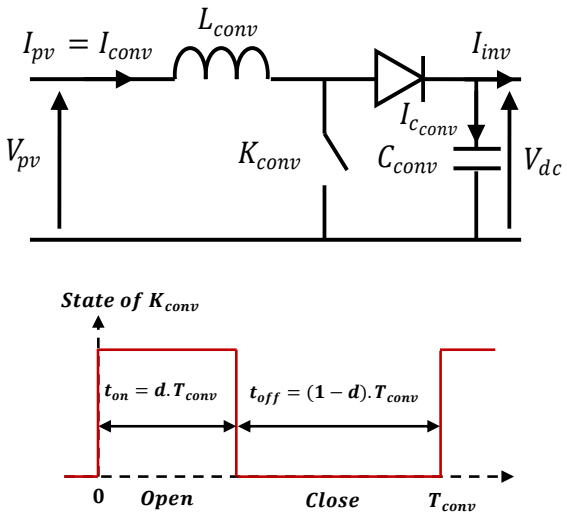

Fig. 4. Circuit topology and operating principle of the boost converter.

During the two complementary time intervals t_{on} and t_{off} in each period T_{conv}, the boost converter can be modelled as follows:

$$\begin{cases} di_{pv}/dt = (v_{pv} - (1-d)v_{dc})/L_{conv} \\ dv_{dc}/dt = (i_{pv}(1-d) - i_{inv})/C_{conv} \end{cases} \quad (4)$$

3. WECS Description and Modelling

3.1. Aerodynamic power captured by the wind generator

According to Betz theorem and Newton's second law, the power extracted from the wind by a turbine is expressed as follows [26, 27]:

$$P_t = \frac{1}{2} C_p \rho S v^3 \tag{5}$$

Equation (6) represents the expression of the C_p for a wind turbine of 1.5 MW which is used in this study (these wind turbine parameters are summarized in [28]):

$$C_p = (0.5 - 0.00167\,(\beta - 2))\sin\left[\frac{\pi(\lambda + 0.1)}{18.5 - 0.3(\beta - 2)}\right] - 0.00184(\lambda - 3)(\beta - 2) \tag{6}$$

3.2. Wind turbine modelling

Considering that the friction coefficients have low and negligible values and that the wind speed distribution is uniform over all the blades, the mechanical model of the wind turbine can be presented as shown in Fig. 5.

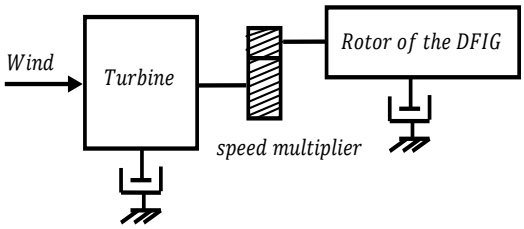

Fig. 5. Simplified mechanical model of the wind turbine.

3.2.1. Wind speed modelling

The wind dynamic properties are very important for the study of a wind energy conversion system because the wind power evolves with the cube of the wind speed in the optimal conditions. Indeed, the wind speed is a three-dimensional vector. However, the direction of the wind velocity vector considered in this model is limited to the horizontal dimension. Consequently, the behavioural model of the wind is simplified considerably. The wind speed *v* is usually represented by a scalar function which varies over time as follows [29].

$$v(t) = v_0 + \sum_{i=1}^{m} A_i \sin(\omega_i t + \varphi_i) \tag{7}$$

where A_i, ω_i and φ_i are respectively, the amplitude, the angular frequency and the initial phase of each spectral component fluctuating.

Table 2 presents the annual mean wind speed in Adrar site subject to the present work which is located in the south of Algeria and it presents the windiest zone in Algeria. It can be seen that the dominant wind speeds in this site are between 3.5 and 7.5 m/s.

Based on the obtained wind speed data of Adrar site, two different wind profiles are shown in Fig. 6. The first profile contains wind gusts and reflects the stochastic nature of the wind speed. On the other, the second profile is a filtered profile with slow dynamics (in this case the fast wind gusts have been filtered from the actual speed). This

last profile is considered and used to pilot the studied WECS in the MPPT mode (the WECS MPPT zone is located almost between 3.5 m/s and 7.5 m/s [28]).

Table 2. Annual mean wind speed in Adrar site (south of Algeria) [30].

Wind class (m/s)	Weibull frequency in (%)	Wind class (m/s)	Weibull frequency in (%)	Wind class (m/s)	Weibull frequency in (%)
0.5	1.7	8.5	8.34	16.5	0.28
1.5	5.20	9.5	6.54	17.5	0.15
2.5	8.20	10.5	4.86	18.5	0.07
3.5	10.58	11.5	3.42	19.5	0.03
4.5	11.85	12.5	2.29	20.5	0.02
5.5	12.07	13.5	1.46	21.5	0.01
6.5	11.39	14.5	0.88	22.5	0.00
7.5	10.05	15.5	0.51	23.5	0.00

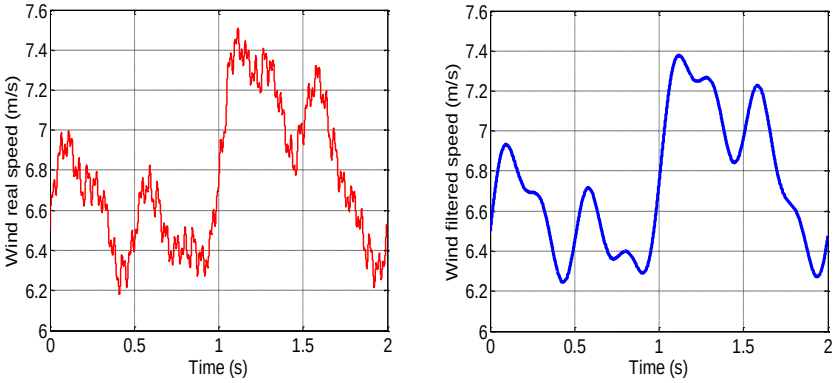

(a) Real profile. **(b) Filtered profile.**

Fig. 6. Different wind profiles.

3.2.2. Turbine model

The aerodynamic torque developed by the wind turbine is as follows [29]:

$$T_{aer} = \frac{P_t}{\Omega_t} = \frac{1}{2\Omega_t} C_p \rho S v^3 \tag{8}$$

3.2.3. Dynamic equation of the generator shaft

By transformation of the mechanical parameters of the turbine to the generator shaft, the shaft dynamic model can be defined by the following equation [28, 29]:

$$J \frac{d\Omega_e}{dt} + D\Omega_e = T_g - T_{em} \tag{9}$$

where: J, Ω_e, D, T_g and T_{em} are respectively, the turbine inertia brought to the generator shaft, the DFIG rotation speed, the turbine friction coefficient brought to the generator shaft, the effect of the turbine torque on the generator shaft and the DFIG torque.

with:

$$J = \frac{J_t}{G^2} + J_e \tag{10}$$

where: J_t, J_e and G are respectively, the turbine inertia, the generator inertia and the multiplier gain.

and:

$$D = \frac{D_t}{G^2} + D_e \tag{11}$$

where: D_t and D_e are the turbine friction coefficient and the generator friction coefficient respectively.

3.3. Relationship between DFIG stator powers and rotor currents

The two-phase reference *(d-q)* frame, which is associated with the stator-rotating field, is used in this paper. The active and reactive powers of the DFIG stator can be obtained based on the Park transformation of the DFIG equations and the stator flux orientation on the *d* axis. Equation (12) presents the expressions of the active and reactive powers based on simplification hypothesis due to the high power rate of the studied wind turbine where the stator resistors are neglected [15].

$$\begin{cases} P_s = -\frac{3}{2} v_s \frac{M}{L_s} i_{qr} \\ Q_s = \frac{3}{2}\left(\frac{{v_s}^2}{L_s \omega_s} - \frac{M}{L_s} v_s i_{dr} \right) \end{cases} \tag{12}$$

where: i_{dr}, i_{qr}, L_s, M, v_s and ω_s are respectively, the rotor current according to *d* axis, the rotor current according to *q* axis, the stator inductance, the mutual inductance, the statorique voltage and the statorique pulsation.

From equation (12), it is clear that the control of the stator active power and reactive power is decoupled, which means that their control can be achieved independently. Indeed, with a constant magnetizing inductance and a powerful network, the P_s power will be directly proportional to the current i_{qr}, and Q_s power will have a linear relation with the current i_{dr} as shown in Eq. (12).

This last equation allows synthesizing the control algorithm of the DFIG produced powers based on the generation of the rotor reference voltages (V_{drref} and V_{qrref}) from the references of the stator powers (P_{sref} and Q_{sref}) using two control loops DFIG, the stator power external control loop and the rotor current internal control loop as shown in Fig. 7.

3.4. Back to back converter control

The DFIG rotor is coupled to the network via a back-to-back AC-DC-AC PWM converter. This converter is composed of the Rotor Side Converter (RSC) and the Grid Side Converter (GSC). These two static converters are controlled to track the

stator-desired powers and to ensure a rotor energy flow in both directions. The GSC and its control block diagram are shown in Fig. 8.

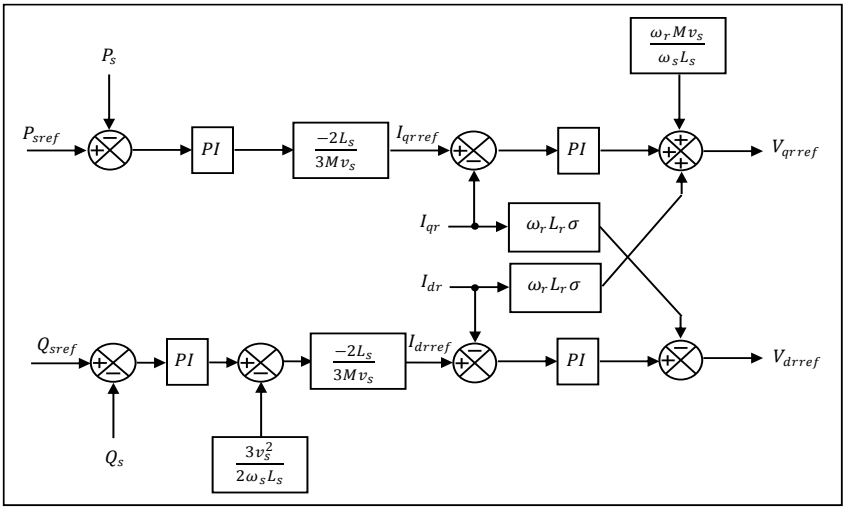

Fig. 7. Control loops of the DFIG stator powers.

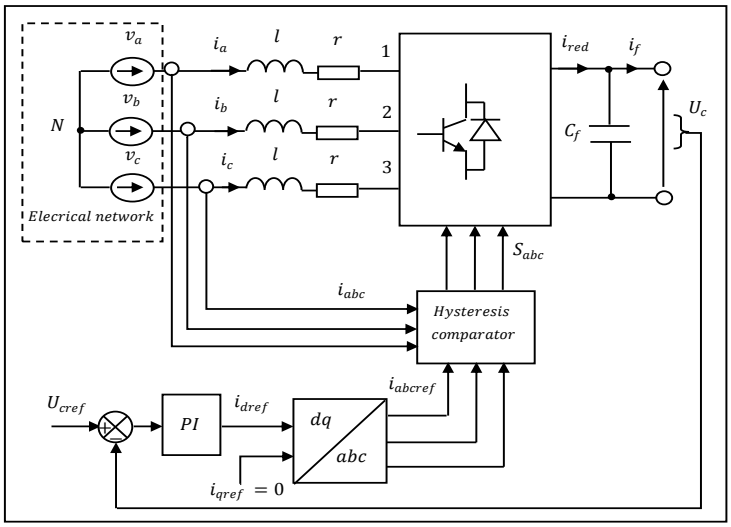

Fig. 8. Control scheme of the GSC.

The GSC control ensures a DC bus voltage stabilization and a unity power factor in the grid side ($i_{qref}=0$). Furthermore, the RSC control ensures the flow of the active power and the reactive power of the WECS through the DFIG rotor, as it is shown clearly in Fig. 9.

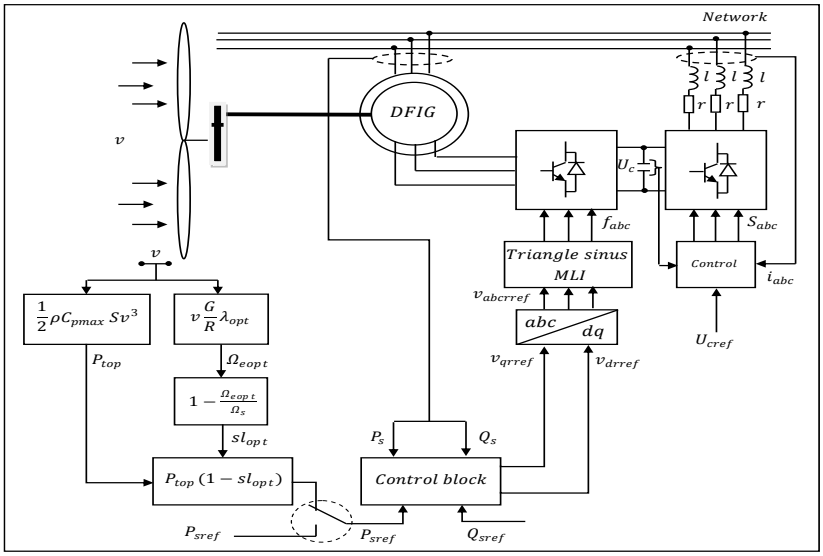

Fig. 9. WECS powers decoupling control.

4. Simulation Results and Discussion

The studied hybrid system in this work is composed of the PVS presented in section 2, and the WECS presented in section 3. These two systems are electrically coupled to be connected to the infinite bus of a powerful balanced three-phase power system network. Initially, it is supposed that the hybrid system operates at its optimal point corresponding to the initial meteorological conditions (T=25°C and g=1000 W/m^2) for the PVS and (v=*6.5 m/s*) for the WECS. In this situation, the PVS and the WECS produce the maximum possible power from the transferred powers of the solar and wind sources. When the temperature and the illumination change according to the profiles presented in Fig. 10 and the wind speed changes according to the profile presented in Fig. 6(b), new power references values corresponding to this new situation will be obtained according to the considered control strategy.

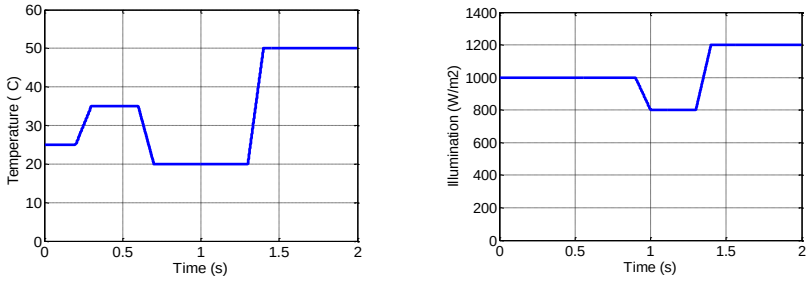

(a) Temperature profile. **(b) Illumination profile.**

Fig. 10. Temperature and illumination profiles applied to the studied PVS (According to Adrar site data).

The obtained simulation results following these meteorological conditions drawn from real data of Adrar site are presented according to each proposed operating mode in the following sections.

4.1. Conventional MPPT mode

The PVS MPPT technique used here is based on the use of a pilot cell implemented in the photovoltaic farm. It is used to estimate on-line the illumination and the temperature and deduce the PV system command value as shown in Fig. 2. The same idea is applied to the wind turbine, where the on-line measurement of the wind speed is used to calculate the maximal active power reference that can be produced by the WECS as shown in Fig. 9.

Figures 11 and 12 show the obtained results of the PVS and the WECS under the standard MPPT mode.

As it can be seen, both systems (PVS and WECS) of the hybrid system have been successfully controlled to operate in the MPPT mode. In fact, the PVS optimal current and voltage track their optimal references for various temperature and illumination levels. On the other hand, it can be noted that the DC bus voltage of the inverter input is maintained within its limits as shown clearly in Fig. 11.

In the WECS side, the stator active power and its reference follow the wind profile applied to the turbine to guarantee the MPPT operation mode Fig. 12. It is noted also that the DC bus voltage remains closer to its reference value of 2000 V as shown clearly in Fig. 12.

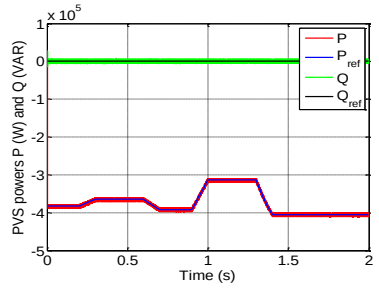

(a) PVS active and reactive powers.

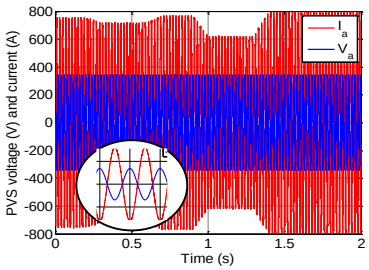

(b) PVS voltage and current.

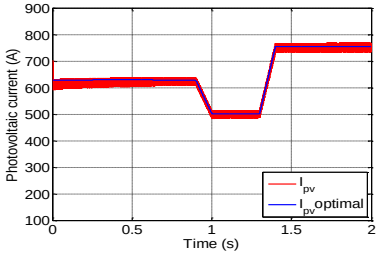

(c) Photovoltaic current.

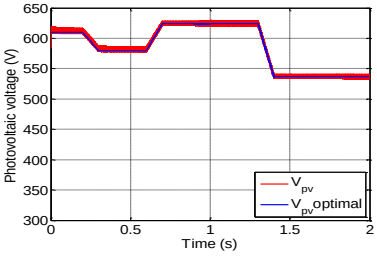

(d) Photovoltaic voltage.

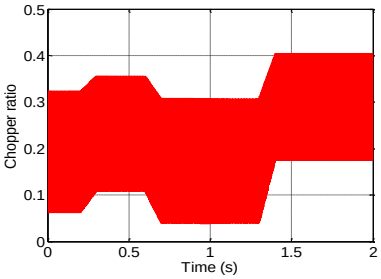

(e) Chopper ratio.

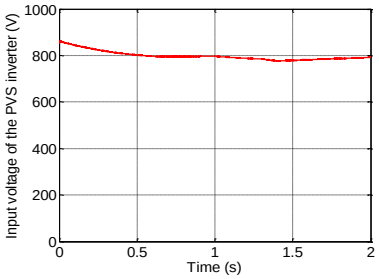

(f) Input voltage of the PVS inverter.

Fig. 11. PVS simulation results in the case of the MPPT mode.

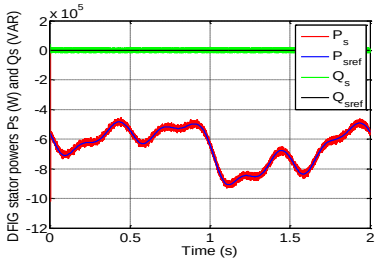

(a) DFIG stator powers.

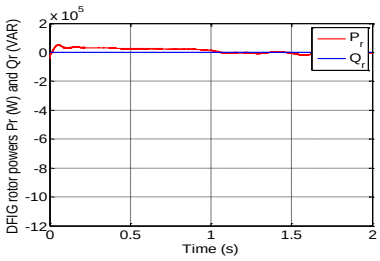

(b) DFIG rotor powers.

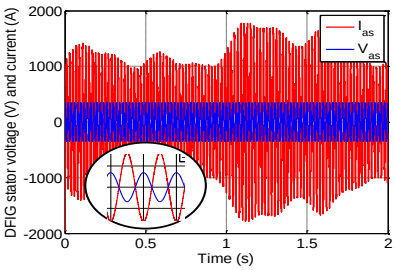

(c) DFIG stator voltage and current.

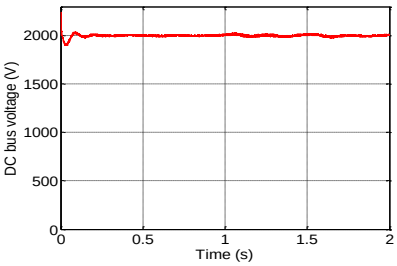

(d) DC bus voltage.

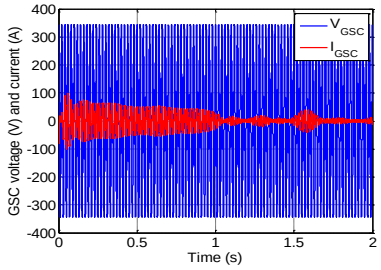

(e) GSC voltage and current.

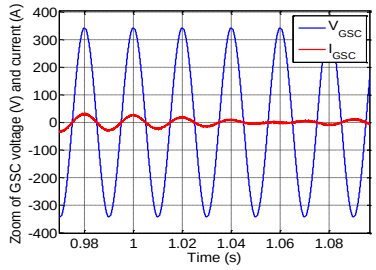

(f) Zoom of GSC voltage and current.

Fig. 12. WECS simulation results in the case of the MPPT mode.

Globally, the hybrid system injects a fluctuated active power of about 1 MW in the grid that may sometimes exceed this value, thanks to the MPPT operating mode of the PVS and the WECS as shown in Fig. 13.

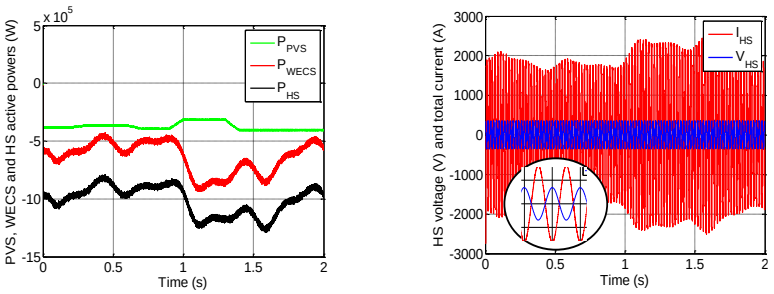

Fig. 13. Simulation results of the HS operating in the MPPT mode.

4.2. Power quality improvement mode

In this mode, the HS is managed to inject a power with improved quality into the power system network according to two techniques. The first technique aims to ensure an improved delivered power according to the of available WECS and PVS powers. The second technique, which is proposed in this paper, is based on a modified MPPT control strategy that guarantees the HS maximum produced power of improved quality.

4.2.1. Improved HS produced power quality based on network-required power

For the same temperature and illumination profiles that are shown in Fig. 10, and for the same wind speed profile which is shown in Fig. 6(b), the total HS produced power follows the required power of the network power system demand according to the weather condition. In this case, the total active power produced by the HS is shown in Fig. 14 (a), while the active powers of the PVS, the WECS and the HS are shown simultaneously in Fig. 14 (b).

It can be noticed that this control technique allows to the hybrid system producing a smooth active power. Initially, the PVS and the WECS provide an active power of 0.8 MW during 1s. Then, they produce a power of 1 MW between 1 s and 1.5 s and finally, a power of 0.9 MW is produced after 1.5 s.

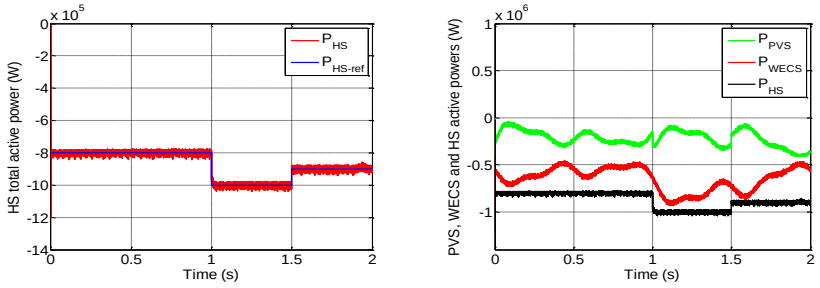

(a) HS global produced power. **(b) Details of the produced powers.**

Fig. 14. Simulation results (production of different smooth power levels).

4.2.2. Modified MPPT mode for power quantity-quality compromise enhancement

To improve the performance of the HS in terms of produced power quantity and quality simultaneously, the previous MPPT operation mode is modified to resolve this dilemma. In this case, a part of the PVS available power is used to compensate the total HS produced power fluctuations resulting from the WECS power fluctuation (due to wind speed gusts). Whereas, another part of the PVS available power is exploited to perform the quantity of the total HS produced power. This can be achieved by considering a slowly and lightly sun illumination during none cloudy days of this Saharan zone comparatively to the rapid and stochastic variation of the wind speed.

In this mode, the PVS reference power is divided into two components. The first one is a fluctuating component constituting the oscillating part of the PVS reference power, which is used to compensate the rapid changes in the power of the WECS that is still operating in the MPPT mode. On the other hand, the second component is constant which will contribute to increasing the total HS produced power. This proposed technique ensures simultaneously the minimization or even the elimination of the fluctuations contained in the total HS produced power and at the same time, maximization of the total HS produced power.

In the next section, the effectiveness of the proposed technique in terms of the HS produced power quantity and quality is evaluated and compared to the two cases of conventional MPPT operating mode and available power operation mode. In the first case, the PVS and the WECS operate in their MPPT mode. Note that the PVS contributes to the production of the total HS power production without taking into account the power fluctuation minimization as shown in Fig. 15. It is obvious (see Fig. 15) that the PVS produces only a constant component (according to the constant weather conditions) which is added to the WECS produced power.

In the second scenario is the guaranteed minimum available power (GMAP) control mode (Fig. 16). In this case, both the PVS and the WECS produce smooth powers, which correspond respectively to available PVS power and to the guaranteed minimum available wind power. In this case, the PVS and the WECS contribute to improving the quality of energy to the detriment of the power quantity comparatively to the first case. In the third scenario (see Fig. 17), the PVS contributes in improving the total HS produced power quality by means of a part of its available power, while enhancing the produced power level by the use of the residual available power. This technique can be applied during the day, to produce different levels of smooth and maximal power according to the weather condition variations.

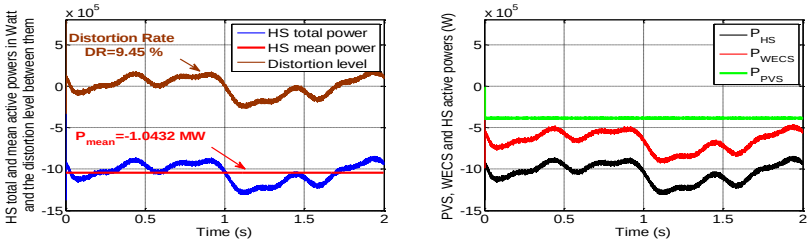

Fig. 15. Simulation results of the classical MPPT mode (with T=25°C and g=1000W/m^2).

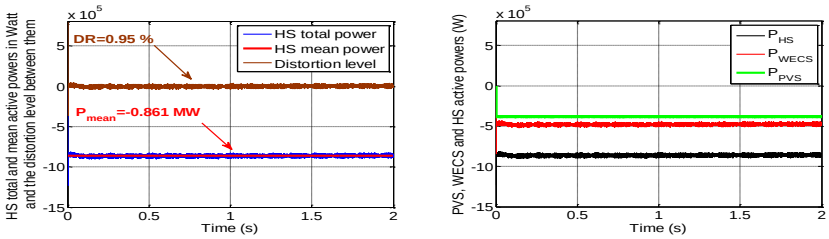

Fig. 16. Simulation results of the guaranteed minimum available power (GMAP) control mode (with T=25°C and g=1000W/m^2).

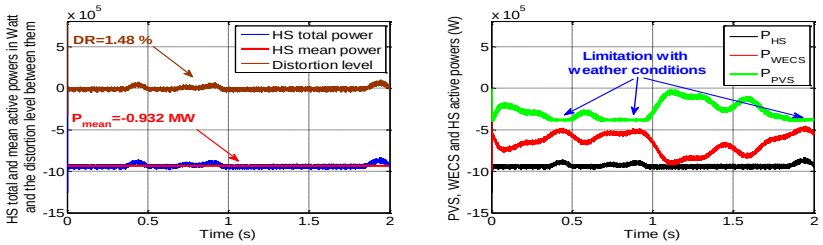

Fig. 17. Simulation results of the modified MPPT mode (with T=25°C and g=1000W/m^2).

To quantify the effectiveness of the three presented control strategies, some results and performance indexes (the HS mean produced power, distortion rate and exploitation level) are calculated and summarized in Table 3.

Table 3. Effectiveness of the three studied strategies.

	Mean Power (MW)	Distortion Rate (%)	Exploitation level versus maximum available power (%)
Classical MPPT mode	-1.043	9.45	100
GMAP control mode	-0.861	0.95	82.55
Modified MPPT mode	-0.932	1.48	89.35

As it can be seen from the results presented in Table 3 that the last case, corresponding to the modified MPPT operating mode, presents the best mode, which allows achieving the required compromise quality-quantity compared to the other control modes. It means that this control mode can ensure for the HS a high - level mean produced power with less fluctuation.

Once more, on the basis of the results presented in Table 3, an economic study is achieved. Indeed, Table 4 presents an estimation of the annual financial benefit that can be reached by applying the proposed control strategy to the HS (it is assumed that the PVS is exploited for an average duration of 6 hours per day and the WECS is exploited for an average duration of 20 hours per day, some hours per day are left to take into account the probability of wind/illumination absence and/or maintenance operation).

Table 4. Financial estimation of the studied HS energy system production profit for the proposed control strategy (Modified MPPT mode).

	Mean Power (MW)	Participation rate in production (%)	Exploitation time per day (h)	Price of electricity/kWh in Algeria (USD)	Annual profit (USD)
PVS	-0.272	29.2	6	≈ 0.33	196,574
WECS	-0.660	70.8	20	≈ 0.33	1 589,940
HS	-0.932	100	/	≈ 0.33	1 786,514

By considering an electricity price per kWh of energy in Algeria of 5 DA (equivalent approximately to about 0.33 USD), the exploitation of the studied HS based on real data obtained on site will ensure a financial benefit of 1 786,514 USD per year. This result will encourage different actors of electrical energy to exploit this studied HS in Algeria. Indeed, this study will motivate different actors in Algeria to reach the government scheduled production level of 13575 MW from PVS and 5010 MW from WECS on the horizon of 2030 [31].

5. Conclusion

In order to resolve the dilemma quantity/quality of energy of renewable energy hybrid systems (composed of a PVS and a WECS) due to the intermittent nature of this kind of energy sources, a modified MPPT control technique has been proposed in this paper. This control strategy has been successfully used to achieve a good compromise between the energy production level and the minimization of the produced energy fluctuation rate. The studied system, composed of a WECS of 1.5 MW of power and a PVS with a rated power of 400 kW, has been presented, studied and simulated on the basis of actual climate data (wind speed, sun illumination and temperature) of the Adrar site (the most important potential in Algeria in terms of wind speed and sun illumination) situated in the south of Algeria. Furthermore, the results of two classical control techniques have been presented in this paper, the first is the conventional MPPT strategy applied to control each system (WECS and PVS) independently. The second strategy is the guaranteed minimum available power (GMAP) control mode based on the mean values of PVS and the guaranteed minimum available power of wind. The modified MPPT proposed control mode presented in this work divides the PVS production into two components: a fluctuating component, which is used to compensate the fluctuations resulting from the WECS produced power, while the second component participates in the overall power production increasing. The simulation results have shown clearly the ability of the proposed technique to resolve the dilemma power quality-power quantity exhibited by this kind of intermittent power systems.

References

1. Somayajula, D.; and Crow, M.L. (2014). An ultra-capacitor integrated power conditioner for intermittency smoothing and improving power quality of distribution grid. *IEEE Transactions on Sustainable Energy*, 5(4), 1145-1155.
2. Badwawi, R.A.; Abusara M.; and Mallick, T. (2015). A review of hybrid solar PV and wind energy system. *Smart Science*, 3(3), 127-138.

3. Ren21 Secretariat (2017). Renewables 2017. Global status report. Retrieved December 28, 2017, from http://www.ren21.net/wp-content/uploads/2017/06/178399_GSR_2017_Full_Report_0621_Opt.pdf.
4. Al Busaidi, A.S.; Kazem, H.A.; Al-Badi, A.H.; and Khan, M.F. (2016). A review of optimum sizing of hybrid PV - Wind renewable energy systems in Oman. *Renewable and Sustainable Energy Reviews*, 53, 185-193.
5. Martin, M.; and Davis, W. (2016). Integration of wind, solar and biomass over a year for the constant production of CH4 from CO2 and water. *Computers and Chemical Engineering*, 84, 313-325.
6. Trifkovic, M.; Sheikhzadeh, M.; Nigim, K.; and Daoutidis, P. (2014). Modeling and control of a renewable hybrid energy system with hydrogen storage. *IEEE Transactions on Control Systems Technology*, 22(1), 169-179.
7. Thounthong, P.; Sikkabut, S.; Mungporn, P.; Piegari, L.; Nahid-Mobarakeh, B.; Pierfederici, S.; and Davat, B. (2015). DC bus stabilization of li-ion battery based energy storage for a hydrogen/solar power plant for autonomous network applications. *IEEE Transactions on Industry Applications*, 51(4), 2717-2725.
8. Shang, C.; Srinivasan, D.; and Reindl, T. (2016). An improved particle swarm optimisation algorithm applied to battery sizing for Stand-alone hybrid power systems. *International Journal of Electrical Power & Energy Systems*, 74, 104-117.
9. Xiong, X.; Chi, K.T.; and Ruan, X. (2015). Bifurcation analysis and experimental study of a multi-operating-mode photovoltaic-battery hybrid power system. *IEEE Transactions on Emerging and Selected Topics in Circuits and Systems*, 5(3), 316-325.
10. Huynh, D.C.; and Dunnigan, M.W. (2016). Development and comparison of an improved incremental conductance algorithm for tracking the MPPT of a solar PV panel. *IEEE Transactions on Sustainable Energy*, 7(4), 1421-1429.
11. Qin, S.; Barth, C.B.; and Pilawa-Podgurski, R.C.N. (2016). Enhancing microinverter energy capture with submodule differential power processing. *IEEE Transactions on Power Electronics*, 31(5), 3575-3585.
12. Wu, B.; Li, S.; Liu, Y.; and Smedley, K.M. (2016). A new hybrid boosting converter for renewable energy applications. *IEEE Transactions on Power Electronics*, 31(2), 1203-1215.
13. Jiang, J.A.; Su, Y.L.; Kuo, K.C.; Wang, C.H.; Liao, M.S.; Wang, J.C.; Huang, C.K.; Chou, C.Y.; Lee, C.H.; and Shieh, J.C. (2016). On a hybrid MPPT control scheme to improve energy harvesting performance of traditional two-stage inverters used in photovoltaic systems. *Renewable and Sustainable Energy Reviews*, 69, 1113-1128.
14. Zhang, L.; Sun, K.; Hu, H.; and Xing, Y. (2014). A system-level control strategy of photovoltaic grid-tied generation systems for European efficiency enhancement. *IEEE Transactions on Power Electronics*, 29(7), 3445-3453.
15. Boutoubat, M.; Mokrani, L.; and Machmoum, M. (2013). Control of a wind energy conversion system equipped by a DFIG for active power generation and power quality improvement. *Renewable Energy*, 50, 378-386.
16. Mahvash, H.; Taher, S.A.; and Rahimi, M. (in press). A new approach for power quality improvement of DFIG based wind farms connected to weak utility grid. *Ain Shams Engineering Journal*.

17. Kamel, R.M. (2016). Standalone micro grid power quality improvement using inertia and power reserves of the wind generation systems. *Renewable Energy*, 97, 572-584.
18. Ram, J.P.; Rajasekar, N.; and Miyatake, M. (2017). Design and overview of maximum power point tracking techniques in wind and solar photovoltaic systems: A review. *Renewable and Sustainable Energy Reviews*, 73, 1138-1159.
19. Kumar, Y.V.P.; and Bhimasingu, R. (2016). A simple modular multilevel inverter topology for the power quality improvement in renewable energy based green building microgrids. *Electric Power Systems Research*, 140, 147-161.
20. Tansi, B.N. (2011). *An assessment of Cameroon's renewable energy resource potential and prospects for a sustainable economic development*. Master Thesis. Faculty of Environmental Sciences and Process Engineering, Brandenburg University of Technology Cottbus, Germany.
21. Motahhir, S.; El Ghzizal, A.; Sebti, S.; and Derouich, A. (2016). Shading effect to energy withdrawn from the photovoltaic panel and implementation of DMPPT using C language. *International Review of Automatic Control (IREACO)*, 9(2), 88-94.
22. Motahhir, S.; El Ghzizal, A.; Sebti, S.; and Derouich, A. (2015). Proposal and implementation of a novel perturb and observe algorithm using embedded software. *Proceedings of the 3rd International Renewable and Sustainable Energy Conference (IRSEC)*. Marrakech, Morocco, 1-5.
23. Kichou, S.; Berges, S.S.; Guglielminotti, L.; Mora-Lopez, L.; and Munoz-Ceron, E. (2016). Comparison of two PV array models for the simulation of PV systems using five different algorithms for the parameters identification. *Renewable Energy*, 99, 270-279.
24. Abd El Satar, M.; Ali, H.; and Elbaset, A.A. (2016). New seven parameters model for amorphous silicon and thin film PV modules based on solar irradiance. *Solar Energy*, 138, 26-35.
25. Motahhir, S.; El Ghzizal, A.; Sebti, S.; and Derouich, A. (2017). MIL and SIL and PIL tests for MPPT algorithm. *Cogent Engineering*, 4, 1378475.
26. Taleb, M. (2017). A grid-connected hybrid wind-solar power system. *Journal of Engineering Science and Technology (JESTEC)*, 12(6), 1697-1708.
27. Ouyang, T.; Kusiak, A.; and He, Y. (2017). Modeling wind-turbine power curve: A data partitioning and mining approach. *Renewable Energy*, 102, 1-8.
28. El Aimani, S. (2004). *Modélisation de différentes technologies d'éoliennes intégrées dans un réseau de moyenne tension*. Ph.D. Thesis. Electrical Engineering. University of Science and Technology of Lille, Lille, France.
29. Boukhezzar, B.; and Siguerdidjane, H. (2009). Nonlinear control with wind estimation of a DFIG variable speed wind turbine for power capture optimization. *Energy Conversion and Management*, 50(4), 885-892.
30. Ksentini, A. (2016). *Gestion et optimisation du site idéal des éoliennes en Algérie pour une zone autonome*. Ph.D. Thesis. Faculty of Technology Department of Electrical Engineering. University of Batna 2, Fesdis, Algeria.
31. Sahraoui, H. (2016). *Modélisation et commande des convertisseurs DC-DC utilisés dans les systèmes photovoltaïques (théorie et expérimentation)*. Ph.D. Thesis. Faculty of Technology Department, University of Batna 2, Fesdis, Algeria.